Geophysical Journal International

Geoelectrical and Seismic Studies of a Mud Volcanic Field: The Salse di Nirano, Italy

Journal:	*Geophysical Journal International*
Manuscript ID:	GJI-14-0790
Manuscript Type:	Research Paper
Date Submitted by the Author:	03-Oct-2014

Complete List of Authors:	Lupi, Matteo; ETH Zurich, Geological Institute Kenkel, Johannes Ricci, Tullio Suski Ricci, Barbara Fuchs, Florian Miller, Stephen

Keywords:	Mud volcanism < VOLCANOLOGY, Volcano seismology < SEISMOLOGY, Hydrogeophysics < GENERAL SUBJECTS

Geoelectrical and Seismic Studies of a Mud Volcanic Field: The Salse di Nirano, Italy

Matteo Lupi[1], Johannes Kenkel[2], Tullio Ricci[3], Barbara Suski Ricci[4], Florian Fuchs*[2], and Stephen A. Miller[5]

[1]ETH Zurich, Geological Institute, Zurich, Switzerland, matteo.lupi@erdw.ethz.ch
[2]Bonn University, Steinmann Institute, Bonn, Germany
[3]Istituto Nazionale di Geofisica e Vulcanologia, Italy
[4]MEMSFIELD, Clamart, France
[5]University of Neuchatel, Centre for Hydrogeology and Geothermics, Nuchatel, Switzerland
*Now at University of Vienna, Department of Meteorology and Geophysics, Austria

1 Abstract

Mud volcanoes are often characterised by elevated fluid pressures deviating from hydrostatic conditions. This near-critical state makes mud volcanoes particularly sensitive to external perturbations. We used the Nirano Mud Volcanic Field as a natural laboratory to test the effects of passing seismic waves generated by distant earthquakes on mud volcanic systems.

We first characterised the subsurface of the Nirano Mud Volcanic Field with a geoelectrical study. Next, we deployed a broadband seismic station within the Nirano Mud Volcanic Field to understand the typical seismic signal generated at depth by mud volcanoes. Seismic records show a background noise below 2 s, sometimes interrupted by pulses of drumbeat-like high-frequency signals lasting from several minutes to hours. To date this is the first observation of drumbeat signal observed in mud volcanoes.

In June 2013 we recorded a M4.7 earthquake event, approximately 60 km far from our seismic station. According to empirical estimations for remote dynamic triggering, the Nirano Mud Volcanic Field should not have been affected by the M4.7 earthquake. Yet, before the earthquake we recorded only weak signals in the 10-20 Hz frequency band while after the earthquake the same frequency band was excited. This lasted for more than 20 minutes with possibly few local microseismic events towards the end of this period.

Our study points out the subsurface structure of the Nirano Mud Volcanic Field and highlights the effects of incoming seismic energy in environments characterised by near-critical conditions at depth.

2 Introduction

Mud volcanoes originate as consequence of fast depositional processes occurring in convergent margins, tectonic belts, submarine slopes, and more generally, where the elevated sedimentation rate impedes fine sediments to dehydrate before being buried. This allows fluids to be retained at depth promoting the formation of isolated geological compartments with elevated fluid pressures. Mud volcanism is recognised around the globe with examples from Trinidad, USA, Azerbaijan, Pakistan, China, Java, and Italy. The proximal region of the Northern Apennines, immediately South of the Pede-Apennines thrust, North Italy, is characterised by several mud volcanic systems aligned along a narrow WNW-ESE trending band that runs sub-parallel to the Pede-Apennines thrust (Figure 1a).

The Nirano Mud volcanic Field (NMVF) is located approximately 20 km SW of Modena, Italy, and sits upon an anticline with a NW-SE axis associated to the Pede-Apennines thrust [Bonini, 2008]. The geological sequence below the NMVF (from depth to surface) consists of Miocene Marnoso Arenacea formations (sandstones and siltstones) at approximately 2 km depth, over-layered by the Ligurian (shales) and the Epi-Ligurian (sandstones, clays stones, and conglomerates) Units. The latter are covered by the gently folded marine and silty clays (Argille Azzurre formation) from Middle Pliocene to Lower Pleistocene. Bonini [2008] suggests that the NMVF is fed by deep fluids seeping from the Marnoso Arenacea formation and percolating along high-angle thrust faults. Fluids accumulate in a shallow reservoir at approximately 0 m a.s.l. within the permeable Epi-Ligurian Units, which is capped by the more impermeable shallow clays. From here fluids migrate vertically through the Marine clays and silty clays reaching the surface at the NMVF.

Figure 1 shows the main geological features of the region, including the distribution of the mud volcanic centres, and an aerial view of the NMVF. The NMVF consists of four main emission centres (cones or ”salse“) aligned along a N55 direction (Figure 1b). Each emission centre is sub-elliptic in shape and may reach up to three meters above the ground. The cones consist of one or more mud vents and the expulsion of fluids is rhythmic and regular within a narrow time-window (i.e. from hours to days). The mud cones are hosted in a subsided area delimited by ring faults that is morphologically similar to a volcanic caldera. Bonini [2008] suggests that the expulsion of thousands of cubic meters of mud over the centuries may have induced subsidence and compaction of the shallower structural levels, promoting the formation of such subsided area.

Onset of mud volcanism is often related to seismic activity, with many examples of earthquakes affecting or triggering mud volcanoes (e.g. Mellors et al. [2007], Manga et al. [2009], Lupi et al. [2013]). Martinelli and Ferrari [1991] highlight that the normal activity of some mud system in northern Italy is periodically interrupted by paroxysmal events. Bonini [2009] points out that the NMVF showed a remarkable increase of fluid emission after the 15^{th} of May 1873 earthquake that occurred at the Pede-Apennines margin, near Reggio-Emilia. In addition, Bonini [2008] reports of a large mud eruption that Plyni describes with sky-scraping flames and smoke visible from approximately 10 km far [Plyni, 6.16 Letters]. According to the Italian catalogue of historic seismic events [Guidoboni, 1989] an earthquake occurred in 91 B.C. close to Modena and hence Plyni's observations may be related to such event.

In October 2012 we conducted a geological field survey of the NMVF observing that after the Emilia seismic sequence (which began on the 20^{th} of May 2012) [Pondrelli et al., 2012], new mud centres in shape of mud ponds, surface mud flows and mud-filled cracks took place within the NMVF. Interestingly, mud outcomes also occurred outside the subsided area that is thought to limit the mud volcanic caldera [Bonini, 2008]. Manga and Bonini [2012] suggest that the Regnano and Puianello mud volcanic centres, NW and SE of NMVF, respectively, and the NMVF responded to the strongest aftershocks of the Emilia seismic sequence. A forester of the natural park of the NMVF was close to one of the cones when the M5.3 Lunigiana earthquake [Samsonov et al., 2013] struck approximately 60 km far from the NMVF on the 21^{st} of June 2013, verbatim: *I was leading a school visit through the park when the earthquake occurred. We were standing nearby the SW mud cone and at first I felt dizzy, with a feeling of spinning head. Then I felt like being above a moving water-mattress.*

Eyewitness records are often too general and not accurate. To avoid qualitative descriptions and ambiguous observations that may lead to misleading triggering thresholds we initiated a geophysical study of the NMVF. In the following, we report the results of a geoelectric survey conducted during

November 2012 at the NMVF. Electrical Resistivity Tomography (ERT) has proven to be a robust and reliable tool to provide realistic, albeit strongly smoothed, images of the spatial electrical resistivity distribution in the shallow subsurface (e.g., Binley and Kemna [2005]). As a consequence, ERT methods have been successfully applied to a wide variety of problems such as hydrogeological and environmental studies (e.g., Binley et al. [2002] Naudet et al. [2004] Revil et al. [2013]), characterization of tectonically active areas [Caputo et al., 2003, Vanneste et al., 2008, Suski et al., 2010]), and most importantly in the given context, to the characterization of mud volcanoes [Istadi et al., 2009, Zeyen et al., 2011, Bessonova et al., 2012].

We also show results from a seismic experiment aimed at understanding the effects of remote earthquakes on the NMVF. For this scope we deployed a broadband seismic station (NIR) within the NMVF (Figure 2). The experiment started in October 2012 (interrupted until June 2013) and concluded in October 2013. The data provide insights about the seismic signal generated by fluids within the NMVF. In addition, we recorded a M4.7 aftershock of the Lunigiana sequence [Samsonov et al., 2013], which allows us to describe the response of the NMVF to incoming seismic energy released by remote earthquakes.

3 Geophysics

In November 2012 we performed a 2D ERT within the NMVF caldera to image the subsurface structure of this area. Because of its sensitivity to porosity, permeability, salinity, and saturation as well as to the presence of clays, ERT is an efficient tool to image the shallow subsurface in general (e.g., Binley and Kemna [2005]) and it is particularly efficient in mud volcanic fields (e.g., Zeyen et al. [2011]). The geoelectrical data were acquired using a Syscal Pro multi-channel resistivity system resistivity system with 48 steel electrodes in dipole-dipole skip-2 and Wenner configurations. The spacing between the electrodes was 2 m for shallower profiles and 5 m for the deeper profiles, which provided a maximum exploration depth between 20 m and 45 m. The wet season and the large amount of high-salinity fluids expelled from the mud vents provided good contacts between the electrodes and the ground. The white arrows in Figure 2 show the direction of the geoelectric profiles. We did not perform any transversal profile across the SW cone as this was already investigated by Accaino et al. [2007]. The longitudinal profile (Figure 3a) is 475 m long and reaches 30 m below the ground surface. To cover the entire longitudinal extension of the caldera, three segments were concatenated to obtain a longer profile with an overlap of 24 electrodes (roll-along). The measured data were then tomographically inverted using Res2DInv to obtain the spatial distribution of the electrical resistivity in the subsurface. The imaging procedure uses smoothness constrained least-squares inversion implemented by quasi-Newton optimisation [Loke and Barker, 1996].

The black triangle in Figure 2 indicates the position of the seismic station deployed from October 2012 to October 2013 (interrupted from November 2012 to June 2013) in the NMVF. We used a Trillium 240s broadband station (sampling rate 100 Hz) equipped with a three-channel Reftek 130 data-logger to acquire the data. We used the ObsPy toolbox [Beyreuther et al., 2010] to process the seismic data. The station was buried 1 m deep, thermally insulated and installed on a concrete plate as no in-place rock crops out within the NMVF. This may affect the amplitude of the recorded seismic signal introducing errors on the estimation of the dynamic stress and strain associated to the passage of the seismic waves. For this reason we do not attempt any estimation of the dynamic stress associated to the passing seismic waves but we limit our observations to a descriptive approach.

4 Data

Figure 3 shows the results of the tomographic inversions of the geoelectric profiles acquired within the NMVF. In the near surface zone (0 – 10 m approx.), very low resistivities (less than 4 Ωm) correspond well with the presence of active vents. At intermediate depths (10 – 20 m), all profiles show intermediate resistivities (4 – 10 Ωm). These can be interpreted as resulting from a water content further below the near-surface (i.e. deeper than 20 m). At depths below about 20 m, all profiles show a broad zone of very low resistivities that is not always directly related to the surface expression of the vents. The conductive regions occur across the entire longitudinal extension of the caldera and are well defined along the NE – SW direction. These observations suggest the occurrence of a rather wide mud mud region approaching the surface to about 20 m deep. Comparison of the obtained resistivities at depth with those at surface indicate that the deep zone contains an important amount of fluids. The fluid transfer from this reservoir to the vents visible at the surface passes through a zone of intermediate resistivity, possibly through relatively narrow conduits before the mud spreads out again in the uppermost 10 m. In the north-easternmost sector of profile 1 (Figure 3a), resistivities increase up to 50 Ωm due to a lower content of fluids and a different lithology. This represents the inferred limits of the subsided area and may be compared to annular cracks and ring faults in volcanic calderas.

The typical seismic signal recorded by the NIR broadband seismic station consists of background noise below 2 s, sometimes interrupted by rhythmic drumbeat high-frequency pulses lasting from several minutes to hours (Figure 4). The drumbeat signal becomes apparent only when using a high-pass filter (i.e. above 5 Hz). The drumbeat signal characterises the higher frequencies and appears on the three components. Each pulse lasts approximately 20 s and it is separated by intervals of low frequency noise lasting from 40 s to 180 s approximately. We identify such a high frequency drumbeat signal irregularly throughout our dataset, with no distinction between day or night hours.

In the late June 2013 the aftershocks of the M5.3 Lunigiana earthquake [Samsonov et al., 2013] were still frequent. We recorded a M4.7 event on the 30^{th} of June (9.8 km deep), approximately 60 km far from the NMVF. Figure 5 shows the spectrogram and the waveform of the M4.7 earthquake at the NIR station. The excitement of the lower frequencies lasted approximately 400 s, including the coda. The earthquake, rich in frequencies between 1 Hz and 2 Hz, caused a maximum vertical and horizontal displacement at the surface of 0.7 mm and 0.48 mm, respectively. However, as the seismometer was deployed upon a concrete plate site effects may have altered these values. Figure 4 shows a seismic event approximately 600 s after the arrival of the seismic waves of the M4.7 event (i.e. at around 900 s in Figure 4). Such local event was not captured by the INGV stations nearby (approximately 20 km far from NIR) and we could not locate the epicentre.

The M4.7 earthquake allowed us to study the effects of incoming seismic energy at the NMVF. Figure 6 compares the seismic signal recorded at the NMVF before and after the M4.7 earthquake (see dashed lines in Figure 4) showing the effects of the incoming seismic energy at the NMVF. We choose time windows of 35 mins because a seismic event occurred at ca. 15:23 UTC obliterated the seismic signal generated by the M4.7 at the NIR station.

The amplitudes of the filtered waveforms are comparable (Figure 6b, f). The spectrum on the left side of Figure 6 shows that the frequency band between 10 Hz and 20 Hz before the M4.7 earthquake is dominated by a weaker signal when compared to the signal recorded after the M4.7 earthquake. The excitement of the high frequencies lasted for approximately 20 minutes, i.e. until the next seismic event occurred.

5 Discussion

Figure 3 shows the geoelectrical profiles and highlights the occurrence of a visible contrast of resistivity at different depths. We find a good correlation between the longitudinal and the transversal profiles. The shallow structure of the NMVF is characterised by low resistivity regions that we interpret as being characterised by high salinity fluids embedded in less conductive regions. The longitudinal profile (Figure 3a) shows shallow reservoirs at about 20 m below the ground surface (ca. 30 m wide and 15 m thick) feeding the mud vents. The most prominent fluid reservoir, located in the central part of the longitudinal profile terminates towards the surface in a channel-like structure. This reservoir seems not to feed any mud vent at the surface (at least in the cross section of this profile). Yet, it has to be considered as part of the complex shallow feeding system. The NW part of the NMVF characterised by two separated mud vents (Figures 1b, 2, and7) is fed by two different shallow reservoirs (Figure 3). Along a NE-SW direction shallow high salinity fluids are not laterally widespread as they are in the NW-SE profiles(Figure 7). Compared to Accaino et al. [2007] our study has a lower resolution but reaches 45 m below the ground surface instead of 20 m. Overall our results agree with Accaino et al. [2007] in identifying channel-like structures in the immediate sub-surface. Accaino et al. [2007] do not identify a lateral variation of the distribution of the shallow fluids as they investigate the sub-surface structure of a single mud cone, and not the entire caldera.

The alignment of the mud cones (Figure 1b) suggests a N55-trending structure along which fluids reach the surface. Fluids flowing through such region reach the subsurface where they accumulate in shallow reservoirs at approximately 200 m a.s.l. (Figure 7). After the Emilia seismic sequence [Pondrelli et al., 2012] new isolated mud extrusions cropped out within the NMVF but also outside the areas around the main mud vents. The mud may have been extruded from the shallow low-resistivity regions trending NW-SE highlighted in the transversal profiles (Figure 3). This would also explain the occasional migration of new mud centres within the caldera as well as the large expulsion of mud from various parts of the caldera after the Emilia earthquake.

The drumbeat signal observed at the NMVF (Figure 4) was previously recorded in volcanoes characterised by dome growth (e.g. St. Helens volcano, USA [Iverson et al., 2006]). Such signal was also observed during dome extrusion at Montserrat volcano [Neuberg, 2000], where with time the drumbeat signal was eventually merging together to generate continuous volcanic tremor. Iverson et al. [2006] suggest that in volcanic environments characterised by dome extrusion the drumbeat signal may be associated to stick-slip motion along the margins of the extruding plug. Kawakatsu et al. [2000] describes long period volcanic (drumbeat) tremor at Aso volcano, Japan. In this case the long period volcanic tremor was proposed to be generated by fluids circulating in the hydrothermal system of the Aso volcano, Japan. We suggest that the drumbeat signal sometimes observed at the NMVF may be associated to slug flow similar to what encountered in volcanic systems (e.g. Vergniolle and Jaupart [1986]). We speculate that gases released from the 10 m deep mud reservoir may migrate as slug flow through channel-like structures similar to the ones observed in Figure 3. The slug flow maintains the pressure high enough to support the expulsion of the hydrocarbon-mud mixture progressively reducing fluid pressure at depth. This leads to compaction of the shallows sediments, which in turn promotes the subsidence of the caldera. We exclude any anthropic origin (i.e. a factory or any sort of pump-induced signal) due to the varying time window that separates each high-frequency peak throughout different pulsing events. In addition, the NMVF is a natural reserve and the closest (private) well would be more than 3 km distant. No pumps were used in the artificial lake located within the NMVF when we identified the drumbeat signal.

Figure 6 shows that the NMVF is affected by incoming seismic energy. The frequency band between 10 Hz and 30 Hz shows a stronger excitement after the passage of the seismic waves generated by the M4.7 earthquake described above. Previous authors [Frehner and Schmalholz, 2010, Korneev, 2011, Maksimov et al., 2011] highlighted the signal produced by waves propagating along fluid filled fractures. Incident body waves may generate secondary seismic waves called Krauklis waves that may fall into resonance emitting a dominant frequency [Frehner, 2014] while propagating back and forth along fluid-filled fractures. Krauklis waves may also be generated by fluid overpressure produced inside the fluid-filled fractures [Ferrazzini et al., 1990]. We propose that the excitement of the frequency band highlighted in Figure 6d may be due to Krauklis waves generated by incoming seismic energy. Alternatively, the effects of the M4.7 earthquake at the NMVF may have been enhanced by the overall geological structure upon which the mud volcanic field resides. Similarly to the LUSI mud volcano, Indonesia, the NMVF sits upon parabolic structure (in this case an anticline [Bonini, 2008]) and may be characterised by an elevated contrast of impedances at depth. The incoming seismic energy generated by the M4.7 earthquake may have then been amplified and focused at depth affecting the deep fluid reservoir [Lupi et al., 2013]. This may have accelerated the slug flow within the high-angle thrust fault leading to the almost continuous excitement of the high frequencies shown in Figure 6.

The M4.7 earthquake that induced the excitement of the high frequencies shown in Figure 6 falls inside the triggering threshold for mud and magmatic volcanoes proposed by Delle Donne et al. [2010] but outside the threshold proposed by Manga et al. [2009]. Delle Donne et al. [2010] use a satellite-derived heat flux inventory for global volcanism to identify earthquake-induced thermal anomalies at active volcanoes. Manga et al. [2009] propose a large database derived from peer-reviewed literature, eyewitness observations and historical records. The most prominent difference between the two triggering thresholds resides in the choice of Delle Donne et al. [2010] to include processes that may not be directly observed at the surface. We measured and investigated other instances of triggered activity (i.e. Lupi et al. [2013], Farias et al. [2014]) falling outside the threshold proposed by Manga et al. [2009] and in agreement with Delle Donne et al. [2010]. This points out that geophysical observations are not always in agreement with eyewitness records. Geological systems may be affected by remote earthquakes without any apparent manifestation at the surface. Therefore we suggest that the term *triggered* should be tight to activated processes that can be witnessed while the more general term *affected* should be used for processes that may be captured with geophysical studies.

6 Conclusions

We have performed a geoelectrical study within the Nirano Mud Volcanic Field and constrained the depth of the fluid-saturated shallow region. This highlighted the widespread occurrence of fluids in the subsurface and provided some constraints to the boundaries of the NMVF caldera. The widespread distribution of fluids within the NMVF may explain the occurrence of new mud centres emerging immediately after the 2012 Emilia seismic sequence.

Our study shows that the typical seismic signal recorded at the NMVF consists of background noise below 2 s, sometimes interrupted by rhythmic drumbeat-like high-frequency pulses that last from several minutes to hours. We suggest that such pulsing events may be associated to slugs of fluids up-welling from the deeply-seated fluid reservoir to the fluid saturated sub-surface. In addition, remote seismic events may excite the frequency band between 10 Hz and 20 Hz promoting the propagation of Krauklis waves or a more vigorous vertical migration of deep fluids favoured by focusing of incoming seismic energy.

An increasing amount of geophysical data point out that small magnitude seismic events may affect geological systems more than what was previously thought. In particular, this work shows that a M4.7 earthquake occurred on the 30^{th} of June 2013 approximately 60 km far from the Nirano Mud Volcanic Field has affected the seismic signal recorded by a broadband seismic station deployed within the Nirano Mud Volcanic Field. We suggest to tight the term *triggered* to processes visible at the surface and using the term *affected* for processes that may be captured by geophysical methods only. Yet, due to the fast evolution of the geophysical methods the triggering threshold currently proposed should be revised with a more quantitative approach.

Acknowledgments

The authors thanks Luciano Callegari and Marzia Conventi for their support and warm welcome. Sebastian Schoppohl is thanked for help in the field. Matteo Lupi was partially supported by Humanitas and the ETH Postdoctoral program.

References

F. Accaino, A. Bratus, S. Conti, D. Fontana, and U. Tinivella. Fluid seepage in mud volcanoes of the northern Apennines: An integrated geophysical and geological study. *Journal of Applied Geophysics*, 63(2):90–101, 2007.

E. Bessonova, S. Bortnikova, M. Gora, Y. A. Manstein, A. Y. Shevko, G. Panin, and A. Manstein. Geochemical and geo-electrical study of mud pools at the mutnovsky volcano (South Kamchatka, Russia): Behavior of elements, structures of feeding channels and a model of origin. *Applied Geochemistry*, 27(9):1829–1843, 2012.

M. Beyreuther, R. Barsch, L. Krischer, T. Megies, Y. Behr, and J. Wassermann. Obspy: A python toolbox for seismology. *Seismological Research Letters*, 81(3):530–533, 2010.

A. Binley and A. Kemna. Dc resistivity and induced polarization methods. In *Hydrogeophysics*, pages 129–156. Springer, 2005.

A. Binley, G. Cassiani, R. Middleton, and P. Winship. Vadose zone flow model parameterisation using cross-borehole radar and resistivity imaging. *Journal of Hydrology*, 267(3):147–159, 2002.

M. Bonini. Elliptical mud volcano caldera as stress indicator in an active compressional setting (nirano, pede-apennine margin, northern Italy). *Geology*, 36(2):131–134, 2008.

M. Bonini. Mud volcano eruptions and earthquakes in the northern apennines and sicily, Italy. *Tectonophysics*, 474(3):723–735, 2009.

R. Caputo, S. Piscitelli, A. Oliveto, E. Rizzo, and V. Lapenna. The use of electrical resistivity tomographies in active tectonics: examples from the Tyrnavos basin, Greece. *Journal of Geodynamics*, 36(1):19–35, 2003.

D. Delle Donne, A. Harris, M. Ripepe, and R. Wright. Earthquake-induced thermal anomalies at active volcanoes. *Geology*, 38:771–774, 2010.

C. Farias, M. Lupi, F. Fuchs, and S. A. Miller. Seismic activity of the Nevados de Chillan volcanic complex after the 2010 M_w8.8 Maule, Chile, earthquake. *Journal of Volcanology and Geothermal Research*, 283(0):116 – 126, 2014.

V. Ferrazzini, B. Chouet, M. Fehler, and K. Aki. Quantitative analysis of long-period events recorded during hydrofracture experiments at Fenton hill, New Mexico. *Journal of Geophysical Research: Solid Earth (1978–2012)*, 95(B13):21871–21884, 1990.

M. Frehner. Krauklis wave initiation in fluid-filled fractures by seismic body waves. *Geophysics*, 79 (1):T27–T35, 2014.

M. Frehner and S. M. Schmalholz. Finite-element simulations of stoneley guided-wave reflection and scattering at the tips of fluid-filled fractures. *Geophysics*, 75(2):T23–T36, 2010.

E. Guidoboni. *I terremoti prima del Mille in Italia e nell'area mediterranea*. Sga, 1989.

B. P. Istadi, G. H. Pramono, P. Sumintadireja, and S. Alam. Modeling study of growth and potential geohazard for Lusi mud volcano: East java, indonesia. *Marine and Petroleum Geology*, 26(9): 1724–1739, 2009.

R. M. Iverson, D. Dzurisin, C. A. Gardner, T. M. Gerlach, R. G. LaHusen, M. Lisowski, J. J. Major, S. D. Malone, J. A. Messerich, S. C. Moran, et al. Dynamics of seismogenic volcanic extrusion at mount St Helens in 2004–05. *Nature*, 444(7118):439–443, 2006.

H. Kawakatsu, S. Kaneshima, H. Matsubayashi, T. Ohminato, Y. Sudo, T. Tsutsui, K. Uhira, H. Yamasato, H. Ito, and D. Legrand. Aso94: Aso seismic observation with broadband instruments. *Journal of volcanology and geothermal research*, 101(1):129–154, 2000.

V. A. Korneev. Krauklis wave in a stack of alternating fluid-elastic layers. *Geophysics*, 76(6): N47–N53, 2011.

M. H. Loke and R. Barker. Rapid least-squares inversion of apparent resistivity pseudosections by a quasi-newton method. *Geophysical prospecting*, 44(1):131–152, 1996.

M. Lupi, H. Saenger, F. Fuchs, and S. Miller. Lusi mud eruption triggered by geometric focusing of seismic waves. *Nature Geoscience*, DOI 10.1038/ngeo1884, 2013.

G. Maksimov, A. Derov, B. Kashtan, and M. Y. Lazarkov. Estimation of hydro-fracture parameters by analysis of tube waves at vertical seismic profiling. *Acoustical Physics*, 57(4):529–541, 2011.

M. Manga and M. Bonini. Large historical eruptions at subaerial mud volcanoes, italy. *Natural Hazards and Earth System Sciences*, 12:3377–3386, 2012.

M. Manga, M. Brumm, and M. L. Rudolph. Earthquake triggering of mud volcanoes. *Marine and Petroleum Geology*, 26(9):1785–1798, 2009.

G. Martinelli and G. Ferrari. Earthquake forerunners in a selected area of northern italy: recent developments in automatic geochemical monitoring. *Tectonophysics*, 193(4):397–410, 1991.

R. Mellors, D. Kilb, A. Aliyev, A. Gasanov, and G. Yetirmishli. Correlations between earthquakes and large mud volcano eruptions. *Journal of Geophysical Research*, 112(B4):B04304, 2007.

V. Naudet, A. Revil, E. Rizzo, J.-Y. Bottero, P. Bégassat, et al. Groundwater redox conditions and conductivity in a contaminant plume from geoelectrical investigations. *Hydrology and Earth System Sciences Discussions*, 8(1):8–22, 2004.

J. Neuberg. Characteristics and causes of shallow seismicity in andesite volcanoes. *Philosophical Transactions of the Royal Society of London. Series A: Mathematical, Physical and Engineering Sciences*, 358(1770):1533–1546, 2000.

Plyni. Plyni the young letters. In *A.D. 62?–c.A.D. 113*, 6.16 Letters.

S. Pondrelli, S. Salimbeni, P. Perfetti, and P. Danecek. Quick regional centroid moment tensor solutions for the emilia 2012 (northern italy) seismic sequence. *Annals of Geophysics*, 55(4), 2012.

A. Revil, M. Skold, M. Karaoulis, M. Schmutz, S. Hubbard, T. Mehlhorn, and D. Watson. Hydrogeophysical investigations of the former s-3 ponds contaminant plumes, Oak Ridge integrated field research challenge site, Tennessee. *Geophysics*, 78(4):EN29–EN41, 2013.

S. Samsonov, M. Polcari, D. Melini, V. Cannelli, M. Moro, C. Bignami, M. Saroli, P. Vannoli, and S. Stramondo. Low magnitude earthquakes generating significant subsidence: the lunigiana case study. In *AGU Fall Meeting Abstracts*, volume 1, page 0936, 2013.

B. Suski, G. Brocard, C. Authemayou, B. C. Muralles, C. Teyssier, and K. Holliger. Localization and characterization of an active fault in an urbanized area in central Guatemala by means of geoelectrical imaging. *Tectonophysics*, 480(1):88–98, 2010.

K. Vanneste, K. Verbeeck, and T. Petermans. Pseudo-3d imaging of a low-slip-rate, active normal fault using shallow geophysical methods: The geleen fault in the belgian maas river valley. *Geophysics*, 73(1):B1–B9, 2008.

S. Vergniolle and C. Jaupart. Separated two-phase flow and basaltic eruptions. *Journal of Geophysical Research: Solid Earth (1978–2012)*, 91(B12):12842–12860, 1986.

H. Zeyen, M. Pessel, B. Ledésert, R. Hébert, D. Bartier, M. Sabin, and S. Lallemant. 3d electrical resistivity imaging of the near-surface structure of mud-volcano vents. *Tectonophysics*, 509(3): 181–190, 2011.

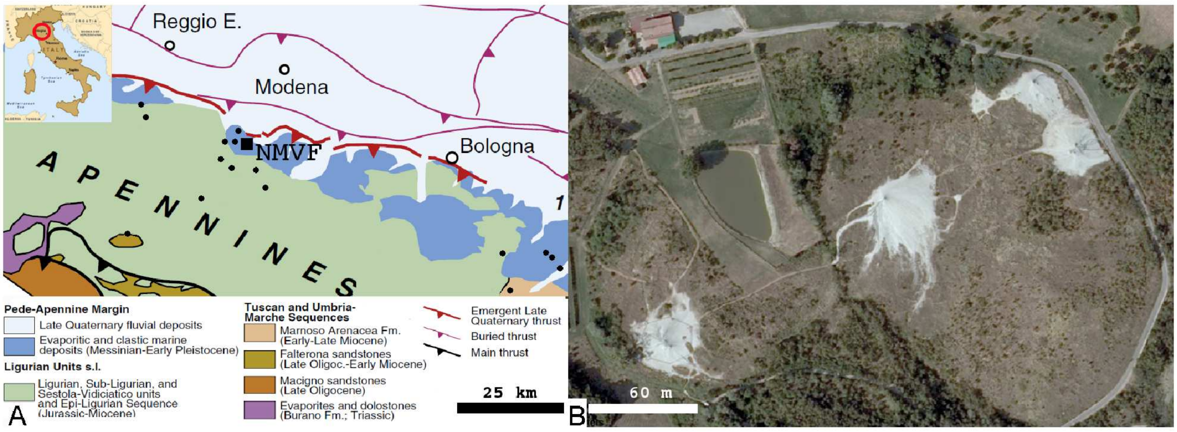

Figure 1: **Geological map of the Pede-Appennine domain and aerial view of the Nirano Mud Volcani Field**. A) Black dots show the location of the mud emissions occurring in the Pede-Appennine margin and the square points out the location of the Nirano Mud Volcanic Field. The Pede-Appenine thrust is marked by the bold red line on the left. B) Top view of the Nirano Mud Volcanic Field showing the four main mud volcanic emission centres.

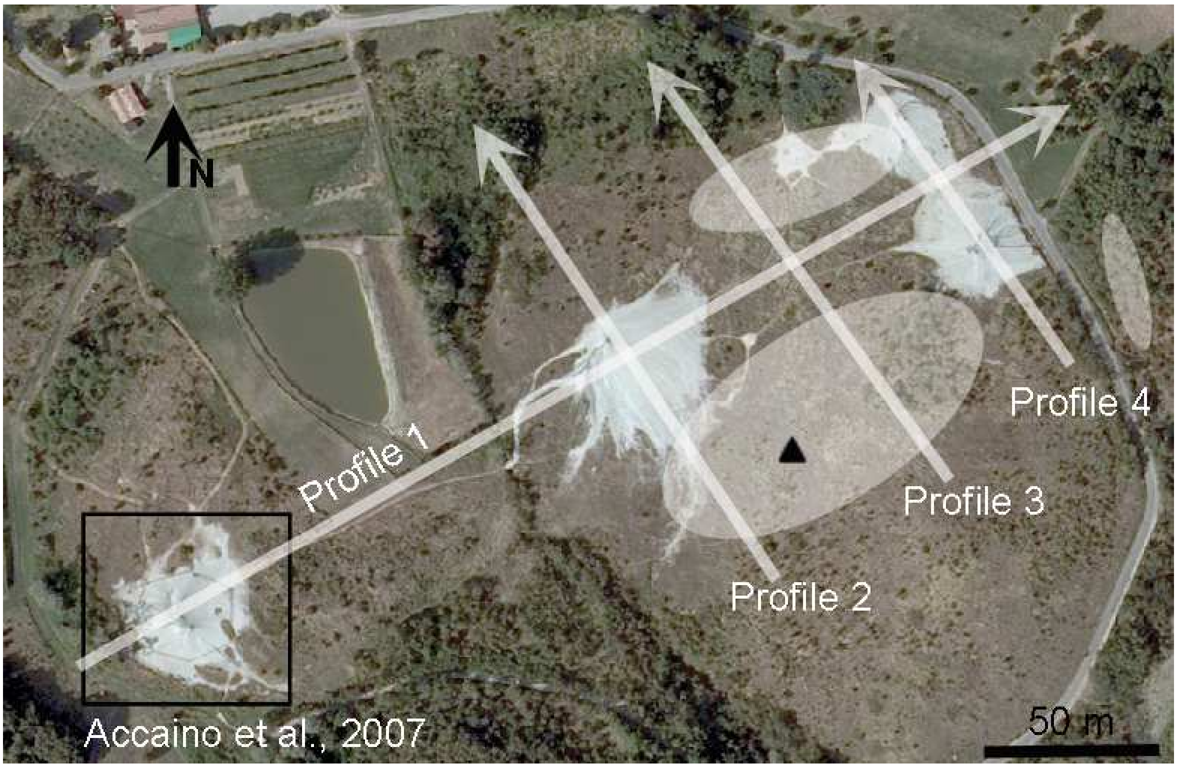

Figure 2: **Direction of geoelectric profiles**. The white arrows indicate the direction of the geolectric profiles presented in this work, the black triangle indicates the position of the seismic station. White shaded areas indicate regions characterised by the expulsion of mud after the 2012 Emilia seismic sequence while the black square points out the region investigated by Accaino et al. [2007].

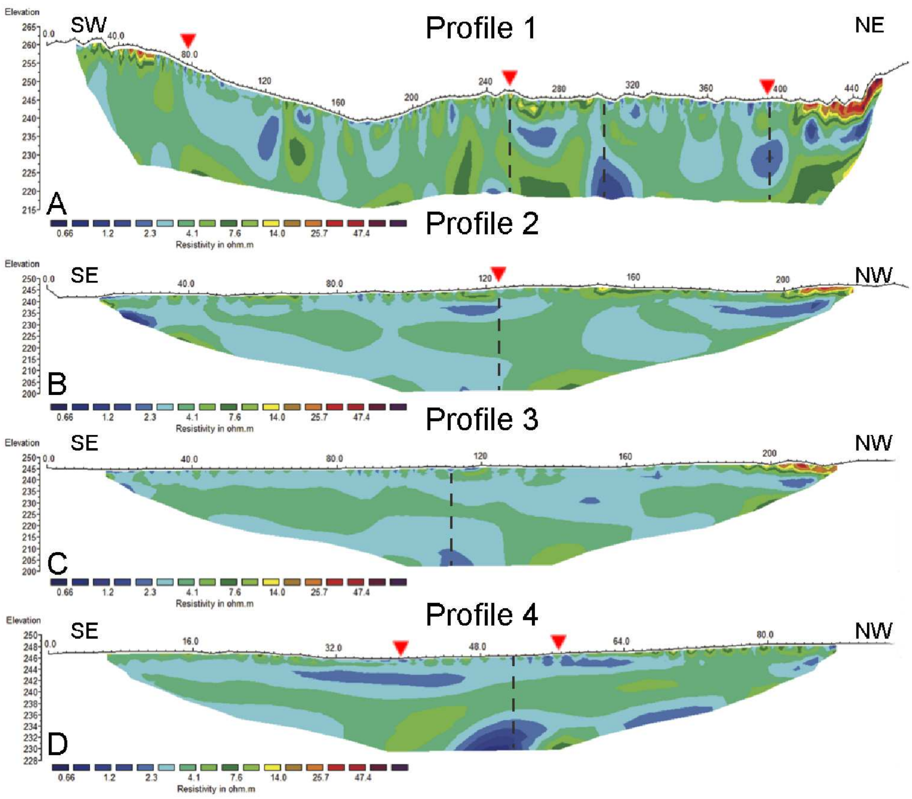

Figure 3: **ERT survey carried out within the NMVF caldera** A) Profile 1, B) Profile 2, C) Profile 3 and D) Profile 4. Refer to Figure 2 for the direction of the profiles. Dashed lines represent the intersection between longitudinal and transversal profiles. Red triangles indicate the location of the mud cones.

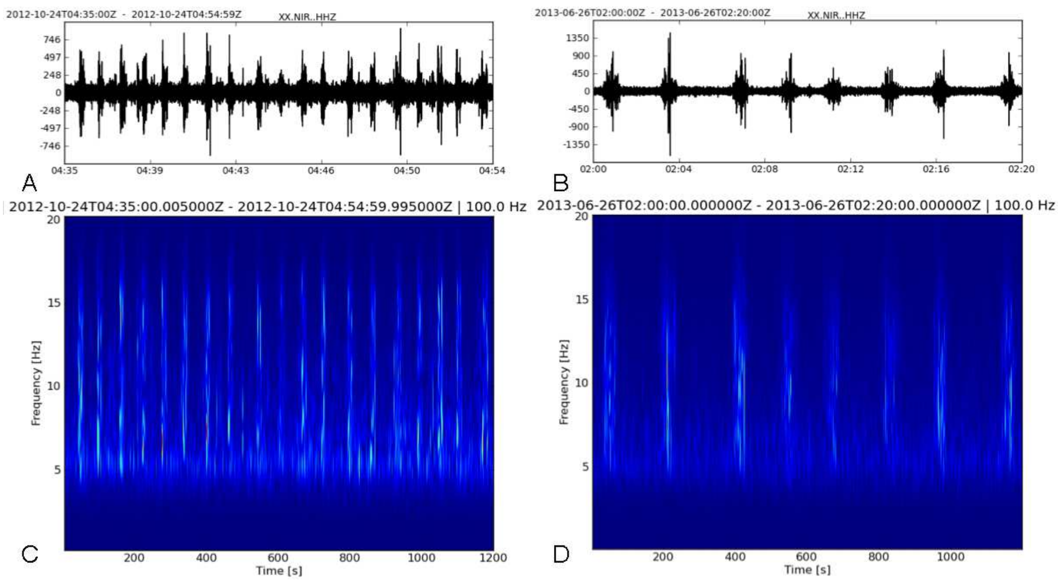

Figure 4: **Waveforms of the drumbeat signal and corresponding spectrogram recorded at NIR station on the 24th of October 2012 and 26th of June 2013.** The signal for the vertical component was bandpassed between 5 Hz and 15 Hz for the Z component. The same signal also appears on the horizontal components.

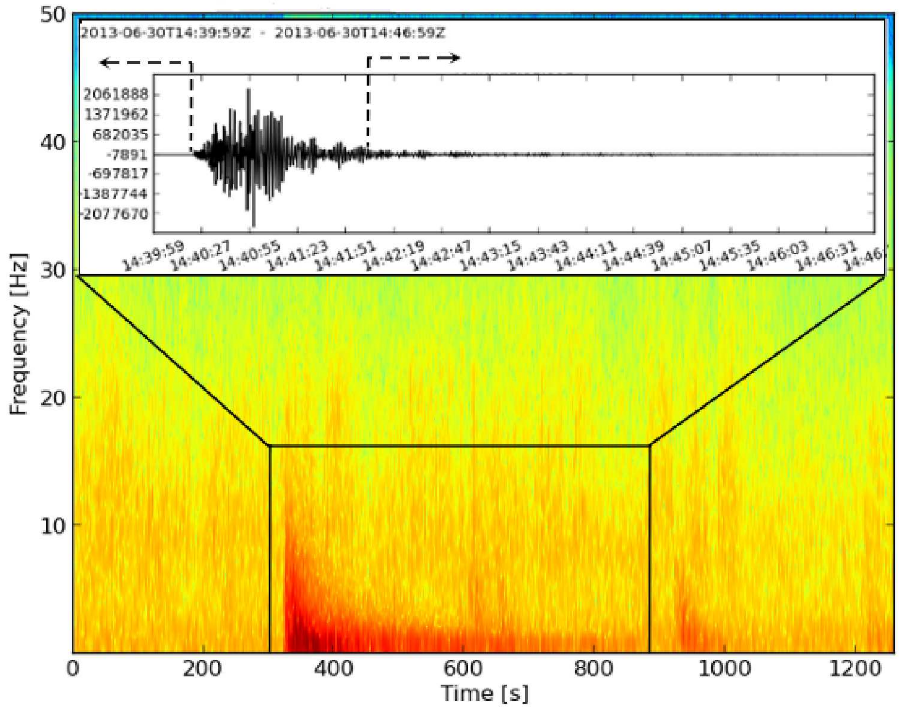

Figure 5: **Spectrogram and waveform of the M4.7 aftershock of the Lunigiana sequence**. The dashed within the waveform plot indicate the time window plotted in Figure 6.

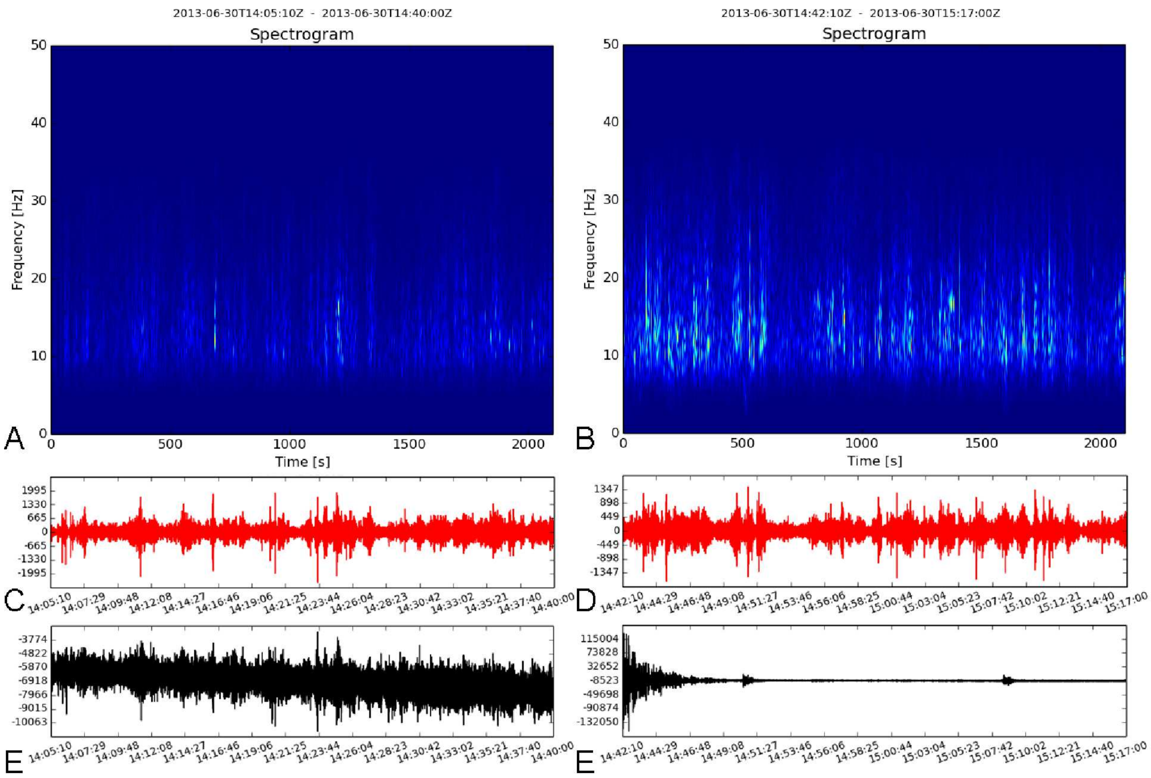

Figure 6: **Comparison between waveforms and spectra before and after the M4.7 aftershock of the Lunigiana earthquake for the vertical component**. The left column shows unfiltered (black waveform) and bandpassed between 10 Hz and 35 Hz (red waveform and spectrum) signal at the NIR station 35 minutes before the earthquake. The right column indicates the same filters for a 35 minutes time window starting 2 minutes after the M4.7 earthquake, i.e. after the coda is dissipated. See dashed lines in Figure 5 for the time windows.

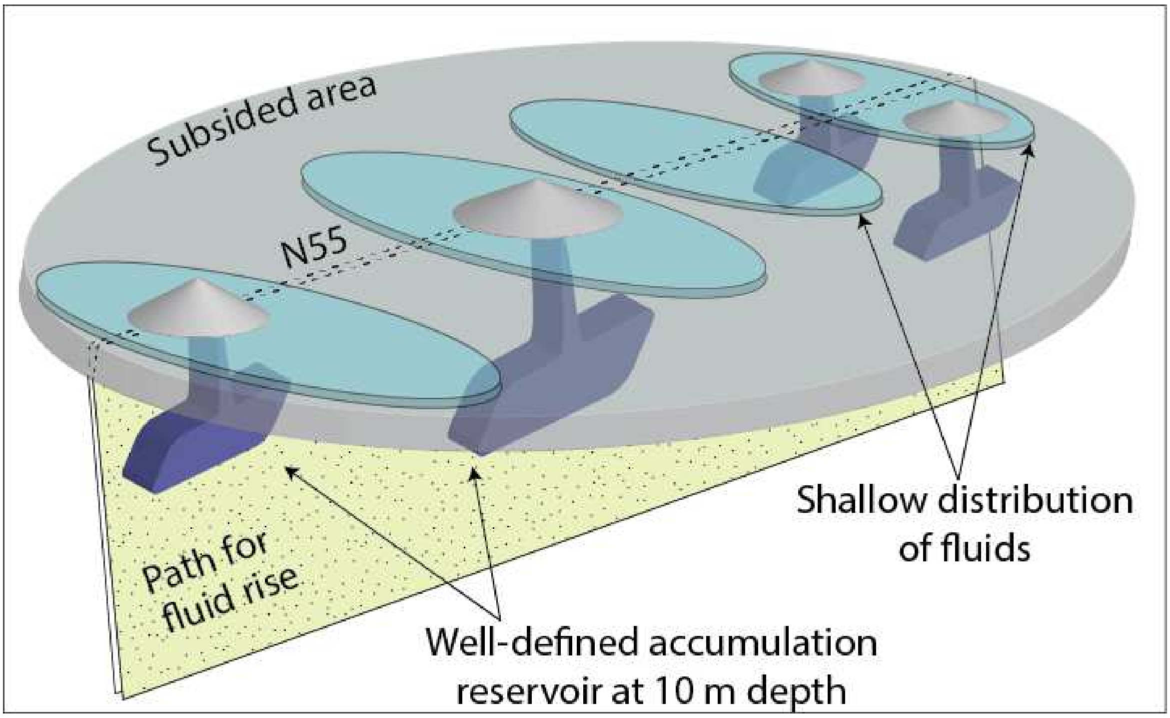

Figure 7: **Cartoon representing the Nirano Mud Volcanic Field**. The mud cones are fed by a proposed up-flow area striking N55. The shallow accumulation reservoirs ($\sim$ 10 m depth) are located within the up-flow zone. When fluids reach the surface they expand laterally along a NW-SE direction.